JOURNAL OF PROPULSION AND POWER
Vol. 10, No. 1, Jan.–Feb. 1994

High-Alpha Vectoring Characteristics of the F-18/HARV

Scott C. Asbury* and Francis J. Capone†
NASA Langley Research Center, Hampton, Virginia 23681

An investigation was conducted in the Langley 16-Foot Transonic Tunnel (16FTT) to determine the multiaxis thrust vectoring characteristics of the F-18 high-alpha research vehicle (HARV). A 0.10-scale model of the F-18 airplane was modified with hardware to simulate the three-vane thrust vectoring system of the F-18/HARV. This investigation was conducted at Mach numbers ranging from 0.30 to 0.70, angles of attack from 0 to 70 deg, and nozzle pressure ratios from 2.0 to approximately 5.0. Results indicate that the thrust vectoring system of the F-18/HARV can generate useful levels of multiaxis thrust vectoring. During vectoring, resultant thrust vector angles were always less than the corresponding geometric vane deflection angle and were accompanied by large thrust losses. Significant external flow effects that were dependent on Mach number and angle of attack were noted during vectoring.

Nomenclature

A/B = afterburning power
C_L = afterbody lift coefficient
$C_{L\max}$ = maximum lift coefficient
C_m = afterbody pitching moment coefficient
$C_{m\delta}$ = longitudinal control power, per degree
C_n = afterbody yawing moment coefficient
C_Y = afterbody side-force coefficient
F = measured axial thrust
F_i = ideal isentropic thrust
F_N = normal force measured by balance
F_r = resultant thrust, $\sqrt{F^2 + F_N^2 + F_S^2}$
F_S = side-force measured by balance
M = Mach number
α = angle of attack
$\delta_{A,D}$ = geometric vector angle of top vanes
$\delta_{B,E}$ = geometric vector angle of lower left vanes
$\delta_{C,F}$ = geometric vector angle of lower right vanes
δ_p = resultant pitch thrust vector angle, $\tan^{-1}(F_N/F)$
δ_y = resultant yaw thrust vector angle, $\tan^{-1}(F_S/F)$

Introduction

MISSION requirements for the next generation multirole fighter may require an aircraft that is capable of operating over a broader range of flight conditions than previously thought possible. To survive air combat engagements, aircraft will require improved handling qualities at high angles of attack, including brief excursions into the poststall region. Several investigations have shown that significant advantages are gained in air combat with the ability to perform transient maneuvers at low speeds and high angles of attack.[1–3] However, maneuverability at high angles of attack can be limited due to degraded stability characteristics and inadequate aerodynamic control power. Techniques for producing large forces and moments by redirecting the engine exhaust flow (thrust vectoring) have been extensively investigated.[4–9] Thrust vectoring provides large control moments that are independent of angle of attack by producing a component of thrust perpendicular to the body longitudinal axis.

The F-18 high-alpha research vehicle (HARV) is an F-18 aircraft modified specifically for flight research at angles of attack up to 70 deg (Fig. 1). One of the HARV modifications to the baseline F-18 was the addition of a multiaxis thrust vectoring system to the conventional axisymmetric exhaust nozzle propulsion system. The thrust vectoring system consists of three externally mounted, deflecting vanes on each nozzle. Multiaxis thrust vectoring is achieved by deflecting these vanes into the exhaust flow.

This article will summarize the results of a wind-tunnel study of the F-18/HARV thrust vectoring system. A 0.10-scale model of the F-18 airplane was modified with hardware to simulate the thrust vectoring system of the F-18/HARV. This investigation was conducted at Mach numbers ranging from 0.30 to 0.70, angles of attack from 0 to 70 deg, and nozzle pressure ratios from 2.0 to 5.0. Model vane deflection angles were varied from −10 to 25 deg. During wind-tunnel tests, the horizontal stabilators were set at −5 deg and the rudders were set at 0 deg.

Apparatus and Model Description

Wind Tunnel

This investigation was conducted in the Langley 16-Foot Transonic Tunnel (16FTT), a single-return, atmospheric wind tunnel with a slotted octagonal test section and continuous

Fig. 1 Photograph of the F-18/HARV in flight.

Presented as Paper 92-3095 at the AIAA/SAE/ASME/ASEE 28th Joint Propulsion Conference, Nashville, TN, July 6–8, 1992; received April 2, 1993; revision received June 9, 1993; accepted for publication June 15, 1993.

*Aerospace Engineer, Propulsion Aerodynamics Branch, Applied Aerodynamics Division, M/S 280. Member AIAA.
†Senior Research Engineer, Propulsion Aerodynamics Branch, Applied Aerodynamics Division, M/S 280. Senior Member AIAA.

air exchange. The wall divergence in the test section is adjusted as a function of the airstream dew point and Mach number; thus, any longitudinal static-pressure gradients in the test section are negligible. The wind tunnel has a continuously variable airspeed up to a Mach number of 1.30. The average Reynolds number per foot ranges from about 1.2×10^6 at a freestream Mach number of 0.20 to about 4.1×10^6 at a freestream Mach number of 1.30.

Model and Support System

An existing 0.10-scale F-18 afterbody jet-effects model was employed for this investigation and is shown in the sketch of Fig. 2 and the photograph of Fig. 3. This wing-tip supported model simulated the F-18 external lines except for the faired over inlets and alteration of the outer wing panels, from 65% of the semispan to the tip, to accommodate the wing-tip support and air supply systems. The wing-tip support system has the unique feature of being able to set the model to a fixed incidence angle relative to the support system. This allows testing of models to high angles of attack while keeping the model at or near the wind-tunnel centerline. Figure 4 shows a photograph of the model at 70-deg angle of attack.

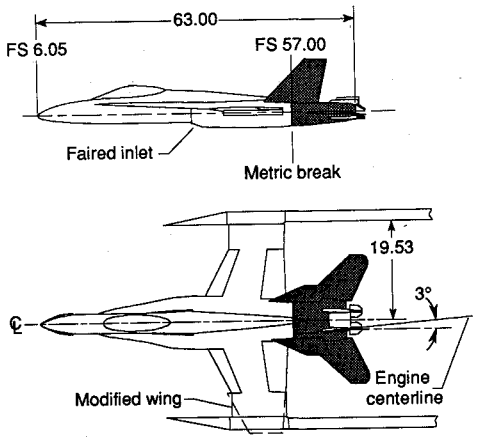

Fig. 2 Sketch of F-18/HARV model; all dimensions in inches.

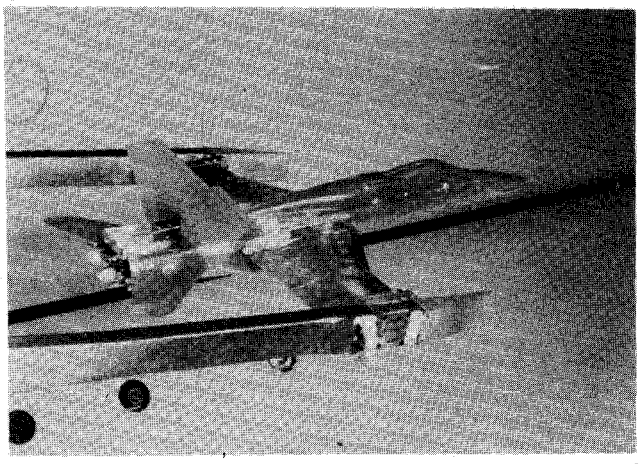

Fig. 3 F-18/HARV model installed in 16FTT at $\alpha = 0$ deg.

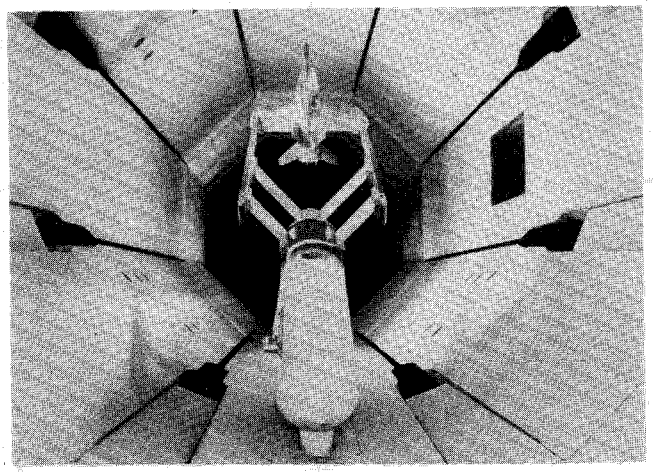

Fig. 4 F-18/HARV model installed in 16FTT at $\alpha = 70$ deg.

The term afterbody, as used in this article, refers to the metric portion of the model (the shaded portion in Fig. 2) on which forces and moments were measured by a six-component strain-gauge balance. The metric break is located at fuselage station (FS) 57.00 and includes the aft fuselage, nozzles (including internal thrust hardware), thrust vectoring system, and empennage surfaces (Fig. 5).

For installation of the F-18/HARV hardware, modifications were made to the model afterbody, starting at FS 66.66. These modifications consisted of removing the divergent section of the F-18 convergent-divergent nozzles and adding the thrust vectoring hardware and a spin chute canister. This installation is shown on the aircraft in Fig. 1 and on the model in Fig. 6. Eliminating the divergent section of the nozzle allowed easier installation of the vane actuation system on the flight test vehicle and minimized the weight increase that resulted from adding the thrust vectoring system to the F-18 aircraft. Two nozzle power settings were investigated which represented a military or dry power setting with a model throat area of 2.20 in.^{2} and an A/B power setting with a throat area of 3.48 in.^{2} As reported in Ref. 10, the results for military and afterburning power nozzles are similar. Therefore, the comparisons presented herein are for the afterburning power nozzle only.

The F-18/HARV thrust vectoring system consisted of three vanes placed asymmetrically about the nozzle exits as shown in Fig. 7. The axial vane position relative to the nozzle exit is shown in Figs. 3 and 5. The radial location of the vanes about the F-18 aircraft afterbody were dictated by existing hardpoints on the aircraft. The size of the top vane (larger than the bottom vanes) resulted from the requirement that the thrust vectoring system produce nearly equal amounts of negative and positive pitch vector angles (nose-up and nose-down moments on the aircraft). A balanced pitch vectoring envelope is essential for improved aircraft stability and post-stall recovery characteristics. The size of the top vane was established in the investigation of Ref. 10.

Earlier static investigations of postexit vectoring concepts and the F-18/HARV concept were performed to optimize the design of the thrust vectoring vanes.[9,10] The results of these investigations determined that the most effective design consisted of vanes with double curvature on the vectoring surface, i.e., axial and radial curvature. The vane planform area is 3.60 in.^{2} for the top vane and 2.63 in.^{2} for each of the two lower vanes. Therefore, the top vane was approximately 27% larger than the other two vanes. The vanes were designed with clipped corners at the trailing edge to allow complete closure of the vanes at maximum vector angles without physical vane interference. During vectoring on the flight test vehicle, only two vanes on either engine are deployed at a given time to eliminate thermal constraints on the aircraft engines. Previous studies of the F-18/HARV thrust vectoring system determined that the vanes do not begin influencing the exhaust flow until they are deployed at 10 deg.[10,11] Therefore, the vane deflection angles investigated were -10 deg (fully retracted), 10, 15, 20, and 25 deg.

Twin-Jet Propulsion Simulation System

High-pressure air was supplied to the twin-jet propulsion simulation system at a constant stagnation temperature of about 530°R at the nozzles. The air was ducted to the model through the wing-tip support booms and the wing. This high-pressure air was then transferred into the metric portion of the model by means of two flow transfer assemblies (Fig. 5).

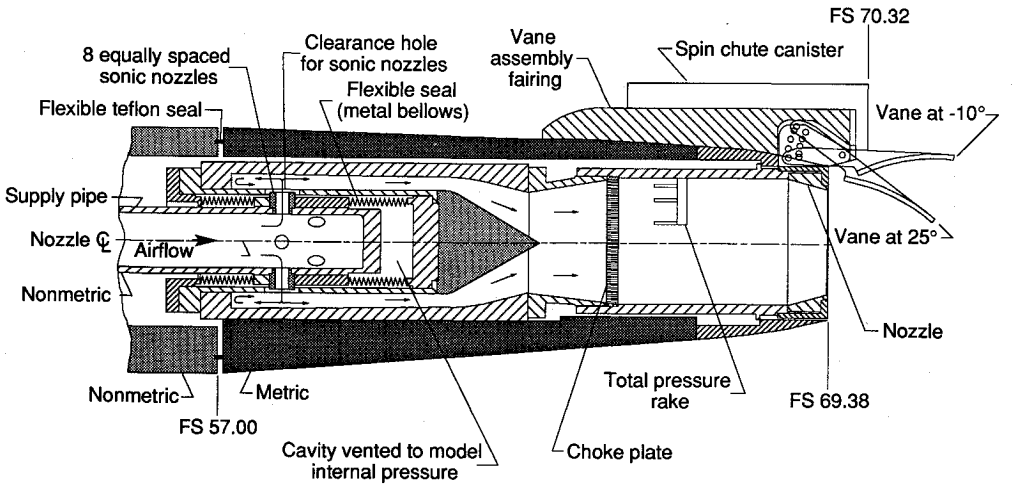

Fig. 5 Details of twin-jet propulsion simulation system; all dimensions in inches.

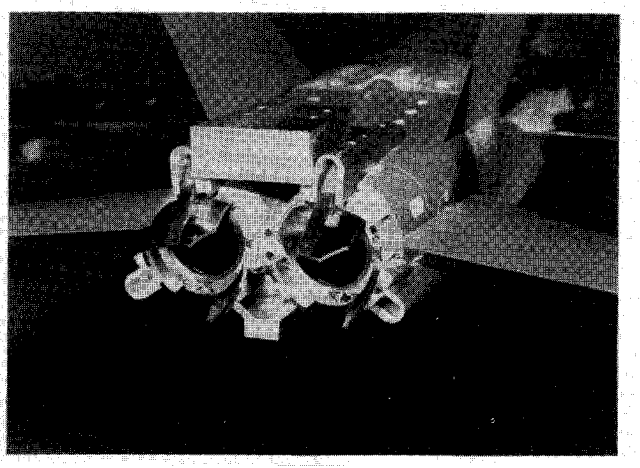

Fig. 6 Vectoring hardware installed on F-18/HARV model.

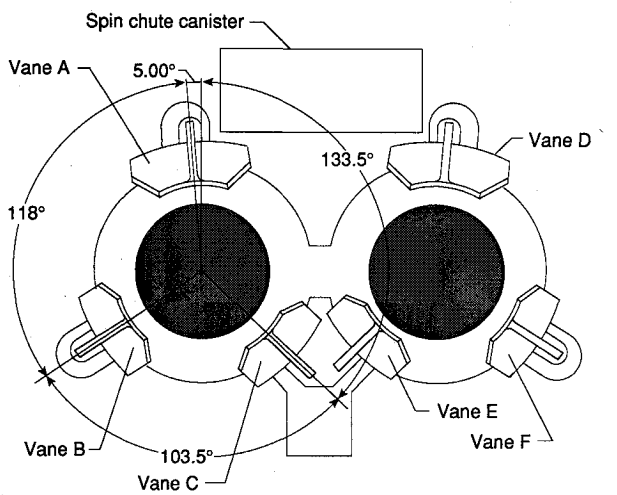

Fig. 7 Thrust vectoring vane position relative to nozzle exit.

Flexible metal bellows are located in each end of the flow transfer assemblies and act to compensate for axial forces caused by pressurization as well as provide a leak-free assembly. Prior to the investigation, extensive jet-on calibrations with ASME nozzles were performed under known load conditions to determine bellows and flow-transfer tare forces.

Transition and instrumentation sections, including choke plates, were attached to each of the flow transfer assemblies. Each instrumentation section contained total pressure and total temperature probes downstream of the choke plate. Thus, ideal nozzle performance parameters calculated from these measurements are free of losses from the transition sections. Weight-flow of the high-pressure air supplied to the exhaust nozzles was determined from a calibrated critical-flow venturi system located in the air line external to the wind tunnel.

Data Reduction

For each data point, approximately 50 frames of data were taken in about 5 s, averaged, and recorded on magnetic tape. Calibration constants were applied to the data to obtain the measured forces, moments, and pressures.

The main parameters used in the discussion of the results at static conditions are resultant thrust ratio F_r/F_i and δ_p and δ_y. F_r was determined from the three force components of the jet measured by the balance. F_i is calculated from the measured weight-flow, total pressure, and total temperature of the jet by assuming isentropic flow. F_r/F_i is used as a measure of the nozzle thrust efficiency or performance.

δ_p and δ_y are the net effective angles through which the flow is turned, projected in the pitch and yaw planes. These angles are calculated from the force components measured by the balance and do not necessarily represent the actual plume angle of the flow.

At wind-on conditions, parameters used in the discussion of results are C_L, C_m, C_Y, and C_n. These coefficients represent the total afterbody forces and moments including thrust components nondimensionalized by freestream dynamic pressure, wing reference area (576 in.^{2}), wing mean geometric chord (13.8 in.), and wing span (39.1 in.). Most of the data presented are plotted as a function of nozzle pressure ratio (NPR) or the model α. The NPR of 4.25, at which the effect of angle of attack was investigated, corresponds to the approximate NPR of the F-18/HARV for flight Mach numbers from 0.30 to 0.70.

Results and Discussion

Static Performance

Static ($M = 0$) performance characteristics that show the effects of vane deflections are presented in Figs. 8–10. Static nozzle performance is presented as F_r/F_i, δ_p, and δ_y.

A matrix of vane deflection angles was tested for the A/B power nozzle at static conditions in order to provide a thrust vectoring envelope. During these tests, at least one vane of each nozzle was always fully retracted, while one or two of the remaining vanes were deployed into the exhaust flow. Part of the matrix of vane deflections tested were divided as follows: a single vane (top) deployed for positive pitch vector angle, two vanes (bottom) deployed for negative pitch vector angle, and two vanes (top and lower left) deployed for combined positive pitch vector angle and negative yaw vector angle. Deflection of the postexit vanes produced useful levels

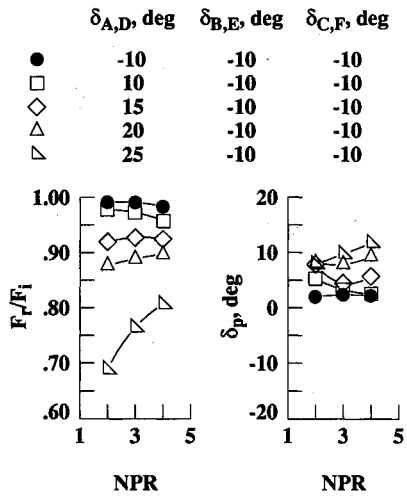

Fig. 8 Effect of vanes *A*, *D* on nozzle static performance.

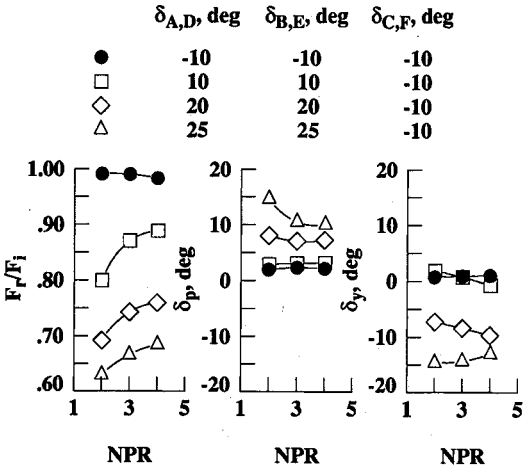

Fig. 9 Effect of vanes *A*, *D* and *B*, *E* on nozzle static performance.

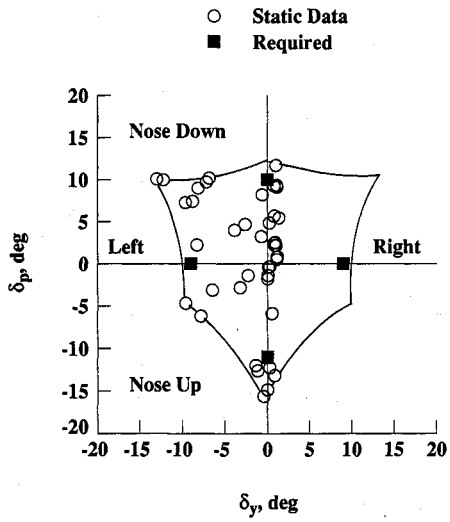

Fig. 10 Static thrust vectoring envelope at NPR = 4.00. Maximum vane deflection angle of 25 deg.

of multiaxis thrust vectoring forces, however, large losses in resultant thrust ratio were noted during vectoring operation. These losses were expected and are a direct result of deploying the vanes into the supersonic jet-exhaust flow. Similar results have been previously reported in Refs. 9 and 10. The thrust losses increased as the vane deflection angle and the number of vanes deployed increased. Although useful levels of thrust vectoring were obtained, the resultant thrust vector angles

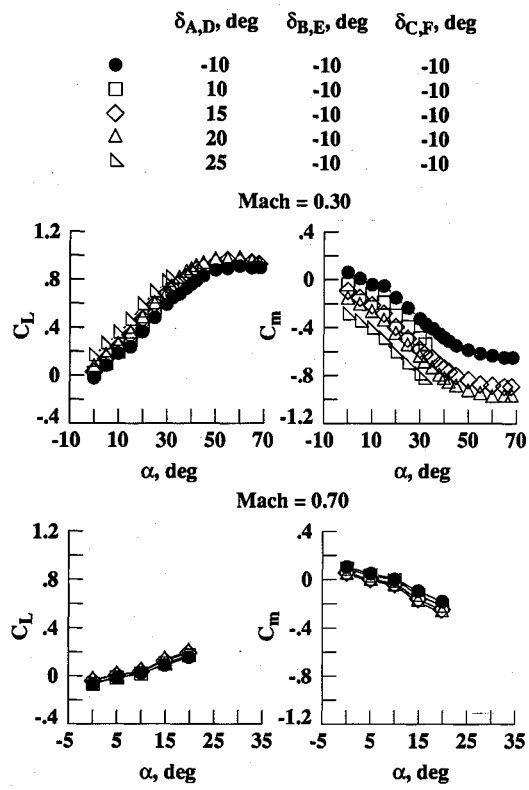

Fig. 11 Effect of vanes *A*, *D* on afterbody aerodynamic characteristics at NPR = 4.25.

generated by the external-vane thrust vectoring system were always less than the corresponding geometric thrust vector angle (physical vane deflection angle). Previous investigations[4,6,8] have studied thrust vectoring concepts which provided a more effective (resultant thrust vector angles approximately equal to geometric vector angles) thrust vector capability. However, the thrust vectoring system for the F-18/HARV aircraft was selected more from schedule, complexity, and cost issues rather than from performance issues.

The results of the parametric vane deployments are summarized in Fig. 10 as a thrust vectoring envelope which was obtained by plotting δ_p against δ_y. Because the thrust vectoring systems of the left and right engines are mirror images of each other, yaw vectoring was only performed in the negative direction during this investigation. The positive δ_y portion of the thrust vectoring envelope was obtained by assuming that the envelope was symmetric in yaw. This envelope illustrates that the net flow turning is always less than the vane deflection angles, as was mentioned previously. The envelope is also slightly asymmetric in pitch, a result of the use of three thrust vectoring vanes positioned asymmetrically around the circumference of the nozzle exit. However, pure pitch or pure yaw vector angles were generated by certain vane deflection combinations, a result indicating that isolated moments could be successfully produced by a three-vane vectoring system. Requirements for the F-18/HARV thrust vectoring system are plotted on Fig. 10 as solid symbols. The requirements fall within the thrust vectoring envelope obtained during this investigation, indicating that the thrust vectoring system provides the required multiaxis vector angles.

Performance at Forward Speeds

Effect of Thrust Vectoring

The effect of thrust vectoring on the total afterbody aerodynamic characteristics (including thrust effects) at Mach numbers of 0.30 and 0.70 is presented in Figs. 11–13. The variation with angle of attack of C_L, C_m, C_Y, and C_n are shown for the F-18/HARV model with either a single vane deployed

(negative pitch) or two vanes deployed (negative pitch, positive yaw). These results are typical of those obtained for other configurations tested in this investigation. The variation of the total aerodynamic characteristics for these two configurations followed expected trends. For example, the increase in C_L with increasing $\delta_{A,D}$ (top vane deflection, Fig. 11) is caused primarily by the jet-lift component of the nozzle resultant thrust and some jet-induced lift. At jet-off conditions, $C_{L_{max}}$ for the afterbody occurs at approximately the same angle of attack as $C_{L_{max}}$ of the F-18/HARV aircraft.[11,12]

Effect of Angle of Attack

The effect of angle of attack on the total afterbody aerodynamic characteristics is shown in Figs. 11–13. The increments in the force or moment coefficients that result from thrust vectoring (deploying one or more vanes into the exhaust flow) remain essentially constant over the entire angle of attack range for all the Mach numbers tested. This lack of angle-of-attack dependency for thrust vectoring is similar to results presented in Refs. 7 and 8.

External Flow Effects

Although the thrust vectoring system of the F-18/HARV is less effective than other vectoring concepts[4,6,8] at static conditions, previous research programs have indicated that thrust vectoring concepts with large deflected surfaces washed by external flow can have large external flow effects on control forces or moments.[6] These external flow effects can, in some cases, substantially improve the flow turning effectiveness of the thrust vectoring system. In order to examine these external flow effects, a breakdown of the individual force components of the total lift and side-force coefficients with two vanes deployed is presented in Figs. 14 and 15 for Mach numbers of 0.30 and 0.70. The data denoted by the circle symbols were obtained at jet-off conditions and represent aerodynamic flap effects, i.e., they contain any lift or side-force generated aerodynamically by the deflected vanes from the nominally undeflected position of −10 deg. The single-line crosshatched region represents the thrust contribution and is determined from results measured at static (M = 0) conditions. The data represented by the squares were obtained at wind-on, jet-on

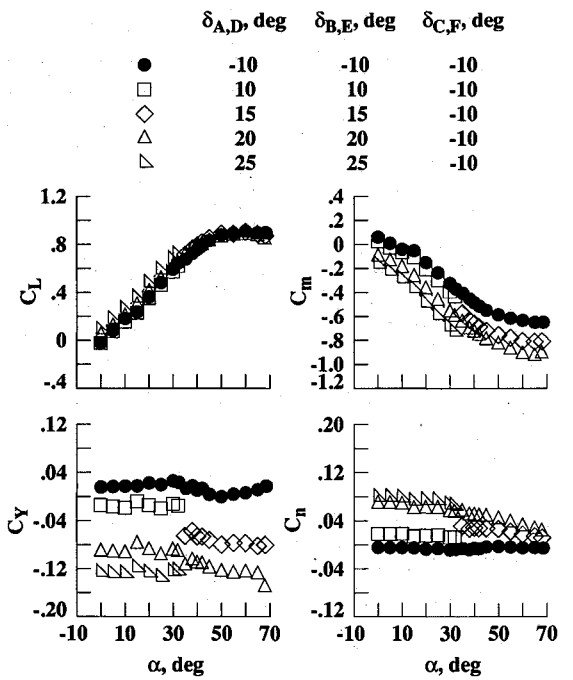

Fig. 12 Effect of vanes A, D and B, E at M = 0.30 and NPR = 4.25.

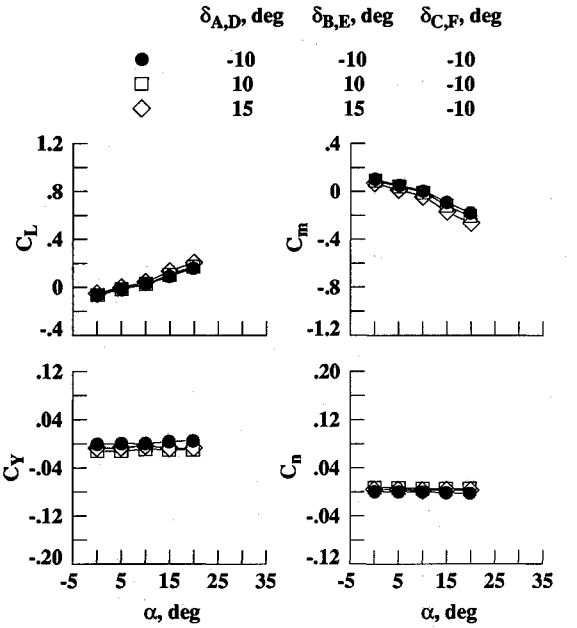

Fig. 13 Effect of vanes A, D and B, E at M = 0.70 and NPR = 4.25.

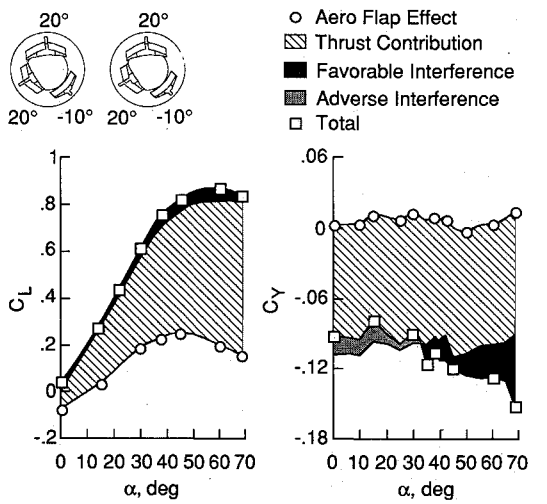

Fig. 14 Breakdown of individual C_L and C_Y force components at M = 0.30 and NPR = 4.25.

conditions and represents the final total value of C_L and C_Y. The difference between the final value of C_L or C_Y and the sum of the aerodynamic flap effect (circles) and the thrust contribution represent a jet-induced interference effect which is caused by the interaction of the external flow with the exhaust plume and the adjacent model surfaces. Jet-induced interference effects result in small favorable increases (dark shading) in C_L for all Mach numbers and angles of attack tested.

At M = 0.30, interference effects reduce the amount of side-force C_Y generated at angles of attack less than 30 deg, and increase C_Y at angles of attack greater than 30 deg. This behavior may be associated with the breakdown of the vortex from the wing leading-edge extension. This breakdown was observed (by natural condensation) at approximately 30-deg angle of attack at M = 0.30 during testing of this configuration, and is substantiated by the results of Ref. 12. At $M \geq 0.70$, favorable interference effects account for approximately 50% of the side-force coefficient generated at 20-deg angle of attack. Similar results were reported in Ref. 7 for a configuration with a pitch vectoring, two-dimensional con-

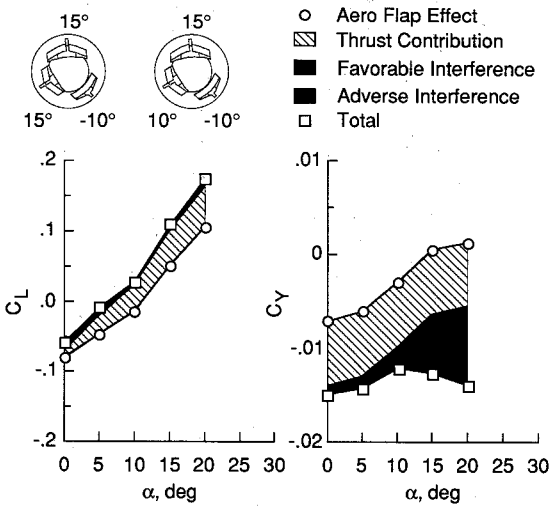

Fig. 15 Breakdown of individual C_L and C_Y force components at $M = 0.70$ and NPR = 4.25.

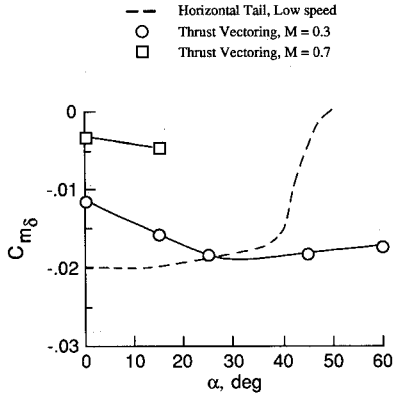

Fig. 16 Comparison of longitudinal control power from thrust vectoring and the horizontal tail.

vergent-divergent nozzle. Since the thrust vectoring envelopes from the static data of Ref. 10 (which does not account for external flow effects) were used to program the flight control system of the F-18/HARV aircraft, significant differences in actual and expected control moments may be noted in flight.

Longitudinal Control Power

A comparison of C_{m_δ} from thrust vectoring and the horizontal tail of the F-18/HARV as a function of angle of attack is presented in Fig. 16. Longitudinal control power from thrust vectoring was evaluated at the Mach numbers noted by symbols at NPR = 4.25. As can be seen, longitudinal control power from the horizontal tail remains relatively constant up to an angle of attack of about 35–40 deg, after which it decreases rapidly to zero control power at 50-deg angle of attack. At $M = 0.30$, control power from thrust vectoring was less than that of the horizontal tail at angles of attack up to 25 deg. However, at angles of attack greater than 25 deg, C_{m_δ} from vectoring was not only greater than C_{m_δ} from the horizontal tail, it remained nearly constant up to an angle of attack of 60 deg. The effectiveness of the thrust vectoring system in producing control forces and moments decreases with increasing Mach number (at constant NPR). This is in contrast to aerodynamic controls which tend to increase in effectiveness with increasing Mach number. The reduction in thrust-generated control power at the higher Mach numbers is a result of a decrease in freestream static pressure and, to a lesser extent, freestream dynamic pressure effects. Because aerodynamic control surfaces are typically sized for low-speed flight, they are generally oversized at higher speeds. Therefore, vectored thrust could be used to supplement aerodynamic controls at low speeds, reducing the required size of aerodynamic control surfaces. Ultimately, this could lead to a reduction in aircraft drag and weight.

Conclusions

An investigation was conducted in the Langley 16FTT to determine the multiaxis thrust vectoring characteristics of the F-18/HARV. A 0.10-scale model of the F-18 airplane was modified with hardware to simulate the thrust vectoring system of the F-18/HARV. The results of this investigation indicate the following conclusions:

1) The three-vane thrust vectoring system of the F-18/HARV can generate useful levels of multiaxis thrust vectoring.

2) During vectored thrust operation, resultant thrust vector angles were always less than the corresponding geometric vane deflection angle. In addition, these resultant vector angles were accompanied by large thrust losses.

3) Longitudinal control power from thrust vectoring was greater than that from the horizontal tail at angles of attack greater than 25 deg at a Mach number of 0.30.

4) Since static thrust vectoring envelopes (which do not account for external flow effects) were used to program the flight control system of the F-18/HARV aircraft, significant differences in actual and expected control moments may be noted in flight.

References

[1]Coates, P., "Investigation of Thrust Vectoring and Post-Stall Capability in Air Combat," AIAA Paper 88-4160, Aug. 1988.

[2]Nguyen, L. T., and Gilbert, W. P., "Impact of Emerging Technologies on Future Combat Aircraft Agility," AIAA Paper 90-1304, May 1990.

[3]Herrick, P. W., "Propulsion Influences on Air Combat," AIAA Paper 85-1457, July 1985.

[4]Capone, F. J., and Berrier, B. L., "Investigation of Axisymmetric and Nonaxisymmetric Nozzles Installed on a 0.10-Scale F-18 Prototype Airplane Model," NASA TP-1638, June 1980.

[5]Mason, M. L., and Berrier, B. L., "Static Investigation of Several Yaw Vectoring Concepts on Nonaxisymmetric Nozzles," NASA TP-2432, June 1985.

[6]Berrier, B. L., "Results from NASA Experimental Studies of Multiaxis Thrust Vectoring Nozzles," Society of Automotive Engineers Paper 881481, Oct. 1988.

[7]Capone, F. J., Mason, M. L., and Leavitt, L. D., "An Experimental Investigation of Thrust Vectoring Two-Dimensional Convergent-Divergent Nozzles Installed in a Twin-Engine Fighter Model at High Angles of Attack," NASA TM-4155, Feb. 1990.

[8]Capone, F. J., Mason, M. L., and Carson, G. T., "Aeropropulsive Characteristics of Canted Twin Pitch-Vectoring Nozzles at Mach 0.20 to 1.20," NASA TP-3060, May 1991.

[9]Mason, M. L., and Berrier, B. L., "Static Performance of an Axisymmetric Nozzle with Post-Exit Vanes for Multiaxis Thrust Vectoring," NASA TP-2800, May 1988.

[10]Mason, M. L., Capone, F. J., and Asbury, S. C., "A Static Investigation of the F/A-18 High Alpha Research Vehicle Thrust Vectoring System," NASA TM-4359, June 1992.

[11]Bowers, A. H., Noffz, G. K., Grafton, S. B., Mason, M. L., and Peron, L. R., "Multiaxis Thrust Vectoring Using Axisymmetric Nozzles and Postexit Vanes on an F/A-18 Configuration Vehicle," NASA TM-101741, April 1991.

[12]Erickson, G. E., "Wind Tunnel Investigation of Vortex Flows on F/A-18 Configuration at Subsonic Through Transonic Speeds," NASA TP-3111, Dec. 1991.